A polydopamine coated polyaniline single wall carbon nanotube composite material as a stable supercapacitor cathode in an organic electrolyte

Xu Wang and Pooi See Lee[a)]
School of Materials Science and Engineering, Nanyang Technological University, Singapore 639798

(Received 6 June 2015; accepted 21 October 2015)

Developing high energy density supercapacitors is of great importance to the transportation, consumer electronics, and micro-grid energy storage sectors. Recently, the development of high voltage organic electrolyte based supercapacitor devices has been gaining much attention. Among them, there is an on-going intense interest in investigating high capacity lithium ion storage anode materials in hybrid supercapacitors. However, developing high capacity cathode materials for high voltage organic electrolyte supercapacitor devices is rarely investigated. The low electrical double layer capacitances of carbon cathode electrodes, which are widely used in current supercapacitor devices, are often the limiting bottleneck. In this contribution, we investigated the electrochemical energy storage behavior of a polyaniline (PANI)-single wall carbon nanotube (SWCNT) composite material in an organic electrolyte as a supercapacitor cathode. The PANI-SWCNT composite exhibits a high specific capacitance of 503 F/g, of which 58.8% of the total capacitance is attributed to the pseudocapacitive and electrical double layer energy storage. The cycling stability of the PANI-SWCNT composite could be further improved by polydopamine (PDA) modification. The PDA with strong adhesion properties is able to prevent mechanical degradation. The PDA modified PANI-SWCNT shows excellent stability with only 5% degradation after 2000 cycles.

I. INTRODUCTION

Supercapacitors are important energy storage devices that can provide transient, but high power output for various machines and devices.[1,2] Electric double layer capacitors (EDLCs) have already been utilized in various applications, such as backup power banks, electricity leveling units, consumer electronics and heavy duty machines.[3] However, the current energy density of commercial EDLC devices can only reach around 10 W h/kg, which makes it hard to penetrate into a larger application market, such as hybrid electrical vehicles. As a result, developing high energy density supercapacitor devices is a topic that has attracted considerable attention.

The evolution of supercapacitor devices from EDLCs to higher energy density supercapacitors can be summarized into two directions.[4] The first direction is to fabricate aqueous electrolyte based asymmetric supercapacitor devices using pseudocapacitive materials and EDLC carbon materials. The second direction is to fabricate organic electrolyte based hybrid supercapacitors using lithium ion battery like energy storage materials and EDLC carbon materials [so called lithium ion capacitor (LIC) or hybrid capacitor]. Extensive research efforts have been exerted in the first direction. However, due to water decomposition in aqueous electrolyte systems, the operation voltages of asymmetric supercapacitors are limited, which deters the improvement in energy density. Recently, organic electrolyte based LIC/hybrid supercapacitors have been brought up as the possible solution for higher voltage and higher energy density.[4] In particular, lithium ion insertion electrode materials with high stability and reasonable capacities are promising electrode candidates for hybrid capacitors, such as MnO_2, V_2O_5, T-Nb_2O_5, TiO_2, $Li_4Ti_5O_{12}$ (LTO), TiP_2O_7, and so on.[5] For example, Naoi et al. recently proposed a nanohybrid material of LTO and carbon nanotubes (CNTs) for hybrid supercapacitors.[4] The energy density of the LIC device composed of LTO// activated carbon is 55 W h/kg at low power density, and it maintains 50% energy density at 6 kW/kg. Meanwhile, it shows excellent long term stability.

However, there is a fundamental obstacle for further enhancing the energy density of hybrid supercapacitors. The energy density of the hybrid supercapacitors could be limited by the low capacitance of prevailing activated carbon electrode materials in the hybrid supercapacitors. Theoretically speaking, the overall capacitance of the hybrid supercapacitor device can be

Contributing Editor: Edward M. Sabolsky
[a)]Address all correspondence to this author.
e-mail: pslee@ntu.edu.sg
This paper has been selected as an Invited Feature Paper.
DOI: 10.1557/jmr.2015.342

https://doi.org/10.1557/jmr.2015.342 Published online by Cambridge University Press

 © Materials Research Society 2015

expressed as $1/C_{total} = 1/C_{-} + 1/C_{+}$. In fact, the overall device capacitance will be limited by the electrode material with lower capacitance. Generally, the capacitance of the activated carbon materials in the organic electrolyte is around 100 F/g (~100 C/g for 1 V testing window),[6] while the capacitance of the lithium insertion electrode is usually higher than 400 C/g (110 mA h/g). In this sense, the energy density of the hybrid supercapacitor device could be further enhanced if there is a high capacitance material to replace the EDLC carbon in the devices. From the past studies,[7] the development of the lithium ion insertion anode materials for the hybrid supercapacitors has been much more successful than the development of a suitable cathode material. There is an urgent need for a better cathode material for the realization of hybrid supercapacitors.

SWCNTs usually have a low specific capacitance due to the lower surface area compared to that of activated carbon. Aligned CNT electrodes have been used in symmetric supercapacitor devices, giving a 2.5 V potential window and a specific capacitance of 65.7 F/g.[8] On the other hand, PANI, a redox active conducting polymer, has been extensively studied in aqueous acid based electrolytes as a supercapacitor electrode.[9–11] Among these, the SWCNT based PANI-SWCNT composite material shows promising electrochemical performance.[9,10] Due to the thin PANI coating, as well as, enhanced conductivity provided by the SWCNT, the PANI-SWCNT composite material shows high specific capacitance over 400 F/g and high rate capability in 1 M H_2SO_4.[9] This value is much higher than those of the carbon electrodes based on the EDLC mechanism. However, the electrochemical stability degradation of PANI is always a concern. The first type of degradation is mechanical degradation, where PANI simply detaches from the substrate. The other one is chemical degradation, which is often the result of over oxidation or over reduction.[12,13] In order to provide a better adhesion of PANI on the substrate, a thin polydopamine (PDA) layer may be an excellent choice. PDA is a bio-inspired polymer from mussels. PDA which has a catechol group shows excellent mechanical adhesion. It has been widely reported that the thin PDA coating is able to provide high mechanical adhesion to various organic and inorganic surfaces.[14] Hence, the use of a PDA coating may be able to provide additional mechanical adhesion for PANI during the electrochemical reaction to reduce the capacitance loss against long term cycling.

In the current work, we propose to use a PDA modified PANI-SWCNT composite material as the high capacitance cathode material in an organic electrolyte for supercapacitor applications. The PDA modified PANI-SWCNT shows a high capacitance of 617.1 F/g at 0.2 A/g and 263.3 F/g at 10.0 A/g with reasonable rate capability that could pair with a lithium insertion negative electrode material. In addition, the PDA modification of the PANI electrode is found to enhance the cycling stability of the cathode.

II. EXPERIMENTAL

The P3-type single wall carbon nanotubes (SWCNTs, 1.0–3.0 at.% carboxylic acid functional group) were purchased from Carbon Solutions Inc., Riverside, CA. The P3-SWNTs have a bundle length ranging from 500 nm to 1.5 μm (~1.0 μm), bundle diameter 4–5 nm. This material is p-doped. The carbonaceous purity of the P3-SWCNTs is higher than 90%. Graphite paper roll is purchased from X2 Labwares (Singapore), with a thickness of 0.15 mm and the sheet resistance is 0.069 Ω/sq. All other chemicals were purchased from Sigma-Aldrich (Singapore) and were used without further purification.

A. Synthesis of the polyaniline (PANI)-SWCNT composite material

In a typical synthesis, 20 mg SWCNTs were first dispersed into a 190 mL 0.5 M sulfuric acid solution with 1 wt% sodium dodecylsulfate under ultrasonication for 1 h. To maintain a thin coating of PANI on the SWCNTs, a low aniline monomer concentration was adopted. Aniline monomer 0.1 mL was injected into the SWCNT suspension and was then cooled to 0 °C using an ice bath under magnetic stirring. A precooled 10 mL of 10 mM ammonium persulfate aqueous solution was added dropwise into the above suspension. The whole system was allowed to stir overnight, and the product was left at room temperature for 3 h. After reaction, the product was collected by centrifugation and was washed with deionized (DI) water and ethanol several times. The product was finally dried by freeze drying. The PANI-SWCNT composite material was labeled as sample PS.

B. Synthesis of the PDA modified PANI-SWCNT composite material

In a typical synthesis, the washed PANI-SWCNT sample was used without freeze drying. The PDA coating synthesis was similar to our group's previous work.[15] The PANI-SWCNT sample was redispersed into a 100 mL pH 8.5 buffer of Tris with continuous stirring. Different amounts of dopamine hydrochloride were added into the above suspensions to give a concentration of 0.1, 0.2, and 0.5 mg/mL, respectively. The reaction was carried out under ambient conditions for 24 h before collecting the samples by centrifugation. The samples were washed with DI water and ethanol several times, and were dried using freeze drying. The samples with a dopamine precursor concentration of 0.1, 0.2, and 0.5 mg/mL were labeled as DPS-1, DPS-2, and DPS-3, respectively.

https://doi.org/10.1557/jmr.2015.342 Published online by Cambridge University Press

C. Structural characterization

The products were characterized using field emission scanning electron microscopy (FESEM, JSM-7600F; JEOL, Tokyo, Japan) and transmission electron microscopy (TEM, JEM-2010; JEOL).

D. Electrochemical characterization

The working electrode slurry was prepared by mixing 85 wt% active material, 10 wt% carbon black, and 5 wt% polyvinylidene fluoride in N-Methyl-2-pyrrolidone (NMP) under continuous magnetic stirring. The mixture was then stirred overnight and the slurry was loaded on the graphite paper by drop casting and dried in an oven at 100 °C overnight. The loading mass of the active material was acquired by measuring the electrode with a microbalance with the accuracy of 0.01 mg. Typically, the loading mass of the active material was around 0.5 mg. The electrochemical tests were performed in a three electrode cell using 1 M $LiClO_4$ in propylene carbonate (PC) as the electrolyte. A piece of Pt was applied as the counter electrode and an Ag/AgCl wire was applied as the reference electrode. The electrochemical tests were conducted using an Autolab PGSTAT 30 potentiostat (Metrohm Autolab, Utrecht, Netherlands). The errors of the electrochemical test results majorly come from the instrumental errors from the microbalance and Autolab. The data errors of material mass (from micro balance) are less than 2% and the errors of the direct electrochemical data are less than 0.01%.

III. RESULTS AND DISCUSSION

A. Structural characterization

The morphologies of different samples were first investigated by scanning electron microscopy (SEM). As shown in Fig. 1(a), the sample PS shows a distinct nanofiber-like network with slight agglomeration at some locations, as indicated by red arrow marks. The variable voids or pores between the nanofiber porous network may be the result of solvent evaporation during the preparation of SEM samples. Under closer observation in Fig. 1(b), in sample PS, the nanofibers are entangled with each other. The diameter of the nanofiber could be observed to be around a few tens of nanometers. Considering the very small diameter of SWCNTs,[16] the larger size of the nanofibers in sample PS indicates the presence of carbon nanotube bundles. In Fig. 1(b), the entangled nanofiber network could be observed more clearly. Such a porous network morphology is expected to be beneficial for the electrolyte penetration as well as the charge in conduction during the electrochemical reaction.

Meanwhile, the amount of dopamine precursor is found to have a profound influence on the final morphology of PDA modified PANI-SWNCT samples. As shown in Fig. 1(c), at a low dopamine starting concentration of 0.1 mg/mL, there is no obvious change in the nanofiber morphology. Partial agglomerates could be also observed as indicated by the red arrow. Under higher magnification of the sample DPS-1, in Fig. 1(d), the nanofibers appear to be a few tens of nanometers in diameter. However, at a higher dopamine starting concentration of 0.5 mg/mL, the sample DPS-3 shows a higher degree of agglomeration as in Fig. 1(e). The nanofibers were closely packed into big particles with diameters over a few micrometers. The merging of adjacent nanofibers can be attributed to the good adhesive nature of PDA.[17] Closer observation of the sample DPS-3 in Fig. 1(f) reveals that the nanofibers are severely agglomerated and the voids between nanofibers are greatly reduced. Meanwhile, the diameter of the nanofibers in sample DPS-3 is larger than those of sample PS and sample DPS-1. This indicates that the excess amount of aniline monomer results in a thick PDA coating on the PANI-SWCNT composite material.

TEM was utilized to further investigate the nanostructure of the sample PS and sample DPS-1, as shown in Fig. 2. As shown in Fig. 2(a), the TEM image confirms the porous network structure of sample PS as observed in Figs. 1(a) and 1(b). Voids with various shapes and diameters could be observed in Fig. 2(a). Under higher magnification, in Fig. 2(b), the SWCNT bundles could be clearly observed in sample PS. This confirms the deduction from the SEM image results. It also can be observed that the polymers are not uniformly coated outside the SWCNT bundles. The thickness of the polymer coating outside the SWCNTs varies at different locations. Meanwhile, the PANI coated SWCNT bundles are buried inside the interconnected PANI.

To prove the existence of PDA as well as PANI in different samples, Fourier transform infrared spectroscopy (FTIR) was carried out for sample PS and sample DPS-1, respectively. As shown in Fig. 3, sample PS corresponds well with the FTIR results from emeraldine salt (1562, 1474, 1298, and 801 cm^{-1}),[18,19] which is a half oxidized protonated state of PANI. Meanwhile, the sample DPS-1 shows the emeraldine base state of PANI (1497, 1307, and 831 cm^{-1}, marked by the red triangles).[20] In addition, the adsorption peaks at 1383 cm^{-1} (marked by red star) could be attributed to the indole ring CNC stretching modes from the PDA.[21] As the PDA coating in the sample was achieved by the polymerization in the pH 8.5 buffer, there is a certain de-doping of the emeraldine salt into the emeraldine base, which was shown in the FTIR results.

The electrochemical properties of different samples were investigated following the structural characterization. Cyclic voltammetry (CV) was first applied to study the electrochemical redox behavior of the different samples. The CV tests were conducted from −0.2 to 0.7 V versus Ag/AgCl in 1 M $LiClO_4$ in the PC

https://doi.org/10.1557/jmr.2015.342 Published online by Cambridge University Press

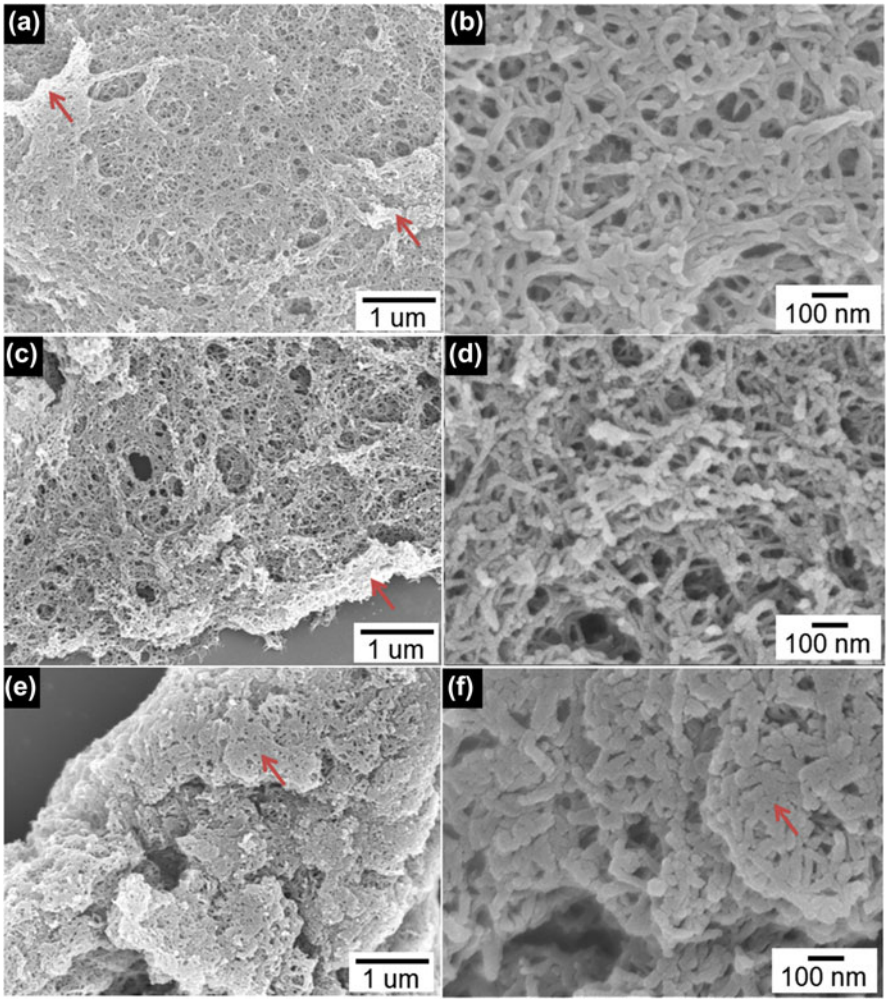


FIG. 1. (a) and (d) SEM images of sample PS at different magnifications; (b) and (e) SEM images of sample DPS-1 at different magnifications; (c) and (f) SEM images of sample DPS-3 at different magnifications.

electrolyte. As shown in Fig. 4(a), the *CV* curves of sample DPS-1 and sample PS both show a pair of broad redox peaks from −0.1 to 0.4 V versus Ag/AgCl. The reaction here could be attributed to the reaction between leucoemeraldine state PANI and emeraldine PANI, which are the insulating state and the half oxidized state.[22] However, the redox reaction peaks between the emeraldine and the pernigraniline are not obvious from *CV* curves, which are typically shown around 0.6 V versus Ag/AgCl in the aqueous acidic electrolyte.[23]

This does not mean there is no transition between the emeraldine state and the pernigraniline state in the samples. The redox current density between the emeraldine state and the pernigraniline state is usually much lower than the leucoemeraldine PANI state and the emeraldine PANI state.[24] Meanwhile, the redox peak current density is also highly dependent on the electrolytes[25] and thickness of the sample,[11] as previously discussed by our group. For the PDA coated SWCNT (PDA-SWCNT) sample synthesized under the same conditions, the *CV* curve shows a slightly distorted rectangular shape. This suggests a predominant electrical double layer capacitance behavior in the PDA-SWCNT sample.

To further understand the electrochemical energy storage behavior of sample PS and sample DPS-1 in the 1 M $LiClO_4$, scan rate dependent Trasatti analysis was carried out at different scan rates.[26,27] This allows us to discriminate charge storage due to easily accessible surfaces (outer, q_o) and the inner surfaces (inner, q_i). The specific charge (q^*) is the total charge exchanged between the electrode and the electrolyte, including both inner and outer charge storage, as shown in Eq. (1).

$$q* = q_i + q_o \quad . \tag{1}$$

The inner charge is diffusion-controlled. Whereas, the outer charge storage is assumed to be not dependent on the scan rates. Thus, the relationship of the charge stored with scan rate can be given as[28]:

https://doi.org/10.1557/jmr.2015.342 Published online by Cambridge University Press

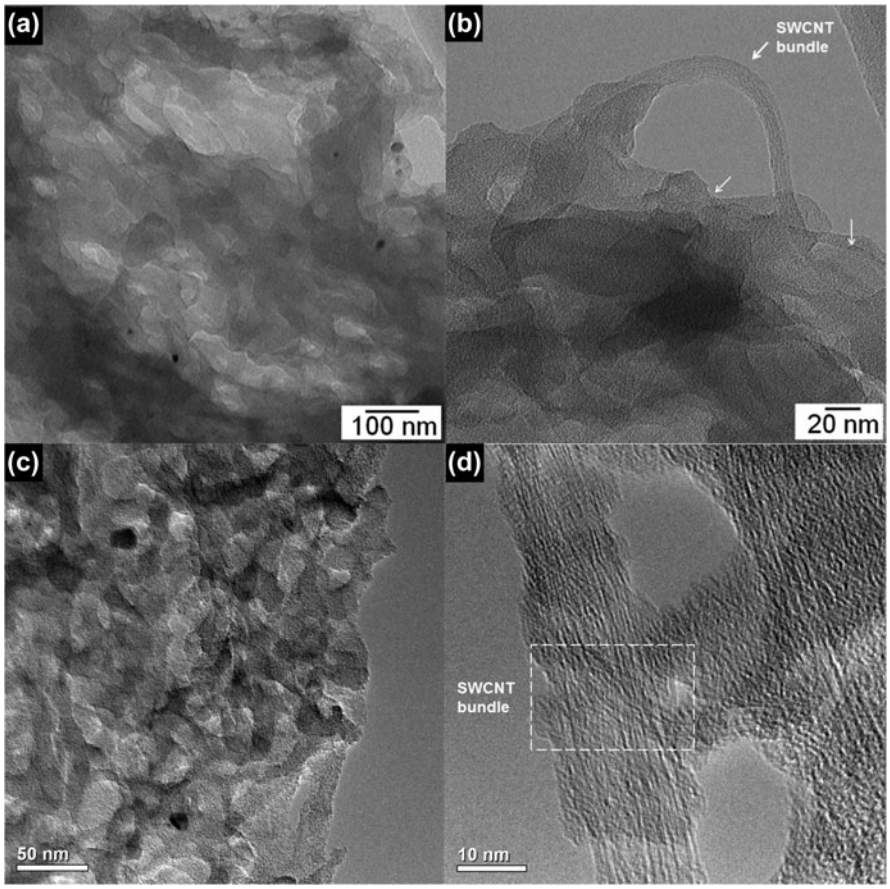


FIG. 2. (a) and (b) are TEM images of sample PS under different magnifications; (c) and (d) are TEM images of sample DPS-1 under different magnifications.

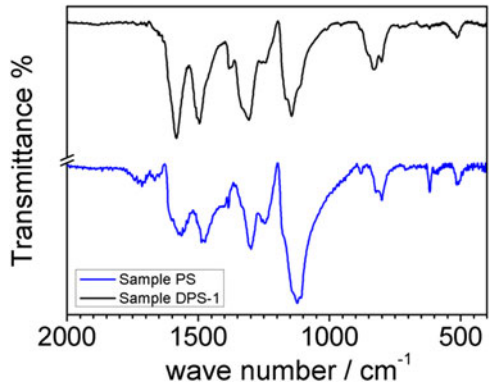


FIG. 3. FTIR spectra of sample PS and sample DPS-1.

$$q* = q_\infty + k/v^{1/2} \quad . \tag{2}$$

When the scan rate $v \to \infty$, q_∞ is the charge stored instantly at the outer and easily accessible surface, which equals to q_o. On the other hand, when the scan rate $v \to 0$, the electrochemically active sites can be fully accessible and q includes both q_i and q_o. To calculate q_o, experiments have been conducted at various scan rates of 2–20 mV/s, as shown in Fig. 4(b). The ratio between surface charge storage and diffusion-controlled charge storage is presented in Fig. S1 (see supplemental material). For sample PS, there is 58.8% of the surface fast charge storage of the total 355.15 C/g charge storage. Meanwhile, for sample DPS-1, there is a slight increase of 3% surface charge storage to 61.8%. Hence, the charge storage behavior of the PANI-SWCNT based composite is a mixture of capacitive and diffusion controlled behaviors. Interestingly, the PDA modification of the PANI-SWCNT composite material improves the capacitive charge storage, as well as, the overall capacity. This point will be elaborated later. On the other hand, taking into account the theoretical capacity of 525 C/g for PANI,[29] there should be a redox reaction between emeraldine and pernigraniline in our case. The disappearance of the corresponding redox peaks in the *CV* measurement may be due to the faster and better electrochemical reversibility[30] between these two states. As a result, it resembles more like capacitive response, which is a typical rectangular *C–V* shape presented in Fig. 4(a).

To further explore the electrochemical behavior of sample PS and sample DPS-1, electrochemical impedance spectroscopy (EIS) was carried out after a few CV

https://doi.org/10.1557/jmr.2015.342 Published online by Cambridge University Press

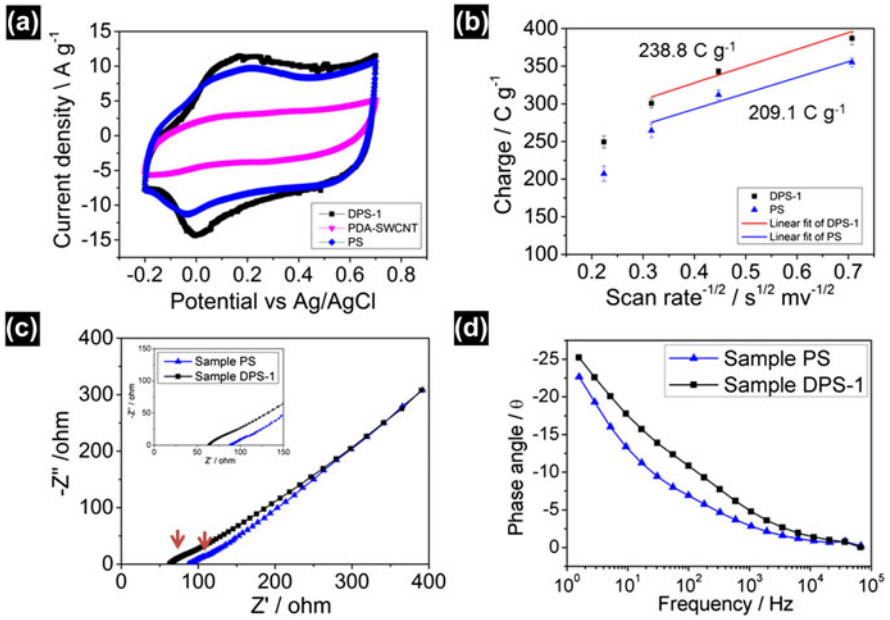


FIG. 4. (a) CV of sample DPS-1, sample PS and sample PDA-SWCNT in 1 M $LiClO_4$ in PC at a scan rate of 2 mV/s; (b) scan rate dependent analysis of sample DPS-1 and sample (the goodness of fit of the gravimetric charges is 0.87 and 0.91 for sample DPS-1 and sample PS respectively); (c) Nyquist plots of sample PS and sample DPS-1, inset is the Nyquist plot at high frequencies; (d) Bode plots of sample PS and sample DPS-1.

cycles, as shown in Fig. 4(c). Generally, there should be a semicircle in the Nyquist plot where the first intercept at the real axis representing the equivalent series resistance (ESR) of the electrodes and the second intercept at the real axis is the electrochemical reaction resistance.[31,32] In our case, there are incomplete semicircles for sample PS and sample DPS-1 as shown in the inset of Fig. 4(c). Nevertheless, the first intercept at the real axis of sample DPS-1 is much smaller than that of the sample PS. This indicates that the equivalent resistance in sample DPS-1 is lower than that in sample PS. It is intriguing that the PDA modification process will lead to the reduced ESR. It could be the result of a more favorable polymer chain alignment through π–π interaction caused by PDA.[33] However, it is noted that the ESR (60–80 Ω) is relatively larger compared to those reports in aqueous electrolyte systems, which is mainly due to the lower conductance of the organic electrolyte. The inferior wettability of the organic solvent on the electrode surface may also be a contributing factor. To reduce the ESR, it will be beneficial to develop a high conductance organic electrolyte using an organic solvent with a higher polarity. For the development of an actual hybrid supercapacitor device, the ESR will be required to be further reduced. On the other hand, in the low frequency range, the angle of the Nyquist plot is smaller than 45°, which indicates the diffusion controlled electrochemical process. It matches well with the scan rate dependent analysis, which shows the diffusion controlled charge storage varied from 38.2 to 41.2% of the total charge. For a more informative analysis of EIS, Bode plots of sample PS and sample DPS-1 are shown in Fig. 4(d). The frequency response of both samples are not typical of the common supercapacitor electrode response, which usually has a characteristic frequency f_0; where, the frequency corresponds to the phase angle at −45°.[34,35] This indicates that the charge storage behavior in the current material system is different from a purely supercapacitive energy storage behavior. Nevertheless, at a given phase angle value, sample DPS-1 shows larger frequency response. This suggests that the electrochemical response of the sample DPS-1 is faster than that of the sample PS.

To evaluate the specific capacitance of different samples, galvanostatic charge–discharge tests were carried out. As shown in Fig. 5(a), the charge–discharge curves of the pure SWCNT sample shows a well-defined triangular shape, which indicates the electrical double layer capacitive behavior of the carbon material in the 1 M $LiClO_4$. Meanwhile, the charge–discharge curves of sample PS, sample DPS-1 and sample PDA-SWCNT show a little deviation from the triangular shape in the potential range between 0.1 and −0.1 V versus Ag/AgCl. There is a small plateau in this range, which corresponds to the transition between the emeraldine state and the pernigraniline state. This indicates a change of the electrochemical energy storage behavior within this range. Therefore, it is possible that the electrochemical reaction between emeraldine and pernigraniline states shows diffusion-controlled kinetics. The specific capacitance of

https://doi.org/10.1557/jmr.2015.342 Published online by Cambridge University Press

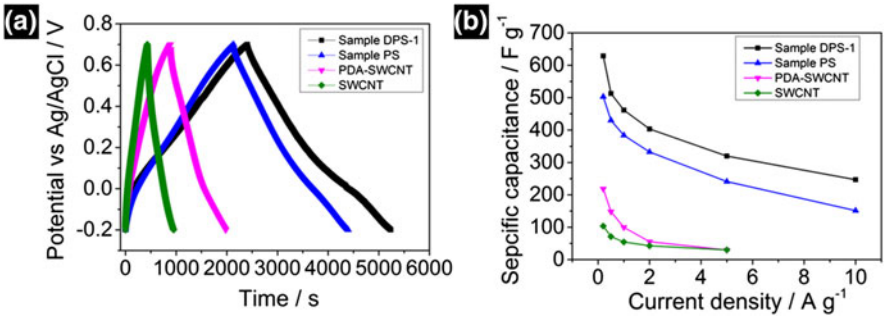


FIG. 5. (a) Galvanostatic charge–discharge curves of sample DPS-1, sample PS, sample PDA-SWCNTs and sample SWCNTs; (b) relationship between specific capacitances and current densities of sample DPS-1, sample PS, sample PDA-SWCNTs and sample SWCNTs.

different samples is calculated from the following Eq. (3) based on galvanostatic charge–discharge tests.

$$C_{sp} = I\Delta t/m\Delta V \quad , \tag{3}$$

where I is the discharge current, Δt is the discharge time, m is the active material mass, and ΔV is the potential window.

The specific capacitance of different samples is shown in Fig. 5(b). For pure SWCNTs, the specific capactance is only 103.7 F/g at 0.2 A/g while it maintains 30 F/g at 5.0 A/g. The relatively inferior rate capability compared to the results in the aqueous electrolyte may be due to the low ionic conductivity of the organic electorlyte.[36] For the PDA coated SWCNTs, however, it shows a significant improvement of specific capacitance to 218.5 F/g at 0.2 A/g. The higher capacitance of PDA coated SWCNT strongly suggests the redox activity of PDA in the 1 M $LiClO_4$. The redox activity may come from the amino group in PDA or the partial transition between dopamine and dopamine-quinone as discussed by Liu et al. in the recent review for PDA.[37] Nevertheless, it is intriguing that PDA shows electrochemical redox activity in the organic electrolyte, which deserves further investigation in the future. For sample PS, owing to the electrochemical redox active PANI, there is an enhancement of specific capacitance compared to the pure SWCNT sample. The specific capacitance of sample PS can reach 503 F/g at 0.2 A/g while it maintains 241.1 F/g at 5.0 A/g. Even when the current density increases to 10.0 A/g, the specific capacitance retains 151.1 F/g, which is 30% of the capacity at 0.2 A/g. This value is much higher than the capacitance of carbon materials tested in the organic electrolyte.[6] On the other hand, the sample DPS-1, however, exhibits 628.9 F/g at 0.2 A/g and 246.7 F/g at 10.0 A/g. The specific capacitances of sample DPS-2 and sample DPS-3 are shown in Fig. S2 (supporting information). Sample DPS-2 shows a similar specific capacitance to sample DPS-1. It reaches 617.1 F/g at 0.2 A/g and 263.3 F/g at 10.0 A/g. Meanwhile, for sample DPS-3, the specific capacitance

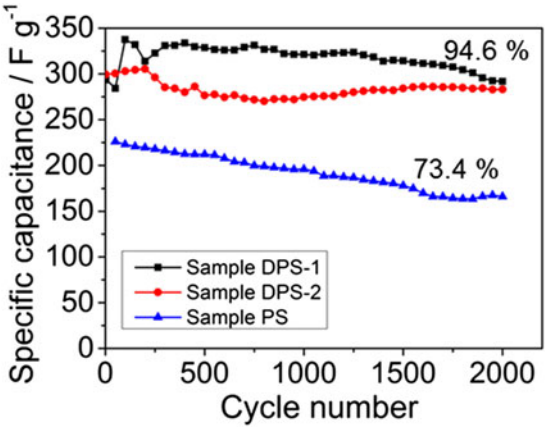


FIG. 6. Long term cycling capacitance retention of sample DPS-1, sample DPS-2, and sample PS at a scan rate of 10 mV/s.

and rate capability are both inferior to sample DPS-1 and sample DPS-2. This could be the result of thick PDA coating that hinders the electrochemical reaction with PANI. With the high specific capacitance and reasonable rate capability, sample DPS-1 and sample DPS-2 are both promising for organic electrolyte based supercapacitors. On the other hand, combining the EIS study in Fig. 4(c), the enhancement of specific capacitance in sample DPS-1 may be due to the following two factors. First of all, the PDA modified sample shows reduced charge transfer resistance during the electrochemical reaction. It facilitates the redox reaction in the PDA modified sample. Secondly, the PDA demonstrated electrochemical activity as shown in Fig. 4(d). The additional redox reaction from PDA contributes to the overall charge storage.

The long term cycling stability is another critical issue for PANI based materials as discussed in the Introduction. To investigate the cycling stability of different samples, continuous cycling voltammetry was carried out for 2000 cycles for different samples. The results are shown in Fig. 6. The sample PS shows quite poor stability during the cycling test, in which the capacitance began to drop since the first cycle. There is only 73.4%

https://doi.org/10.1557/jmr.2015.342 Published online by Cambridge University Press

capacitance retention after 2000 cycles. After employing the PDA modification, the cycling stability of sample DPS-1 is improved as shown by the black curve in Fig. 6. The capacitance of sample DPS-1 was stable after 1000 cycles; however, it experienced a fast degradation after that, especially in the final 500 cycles. The capacitance retention is 80.7% after 2000 cycles. This result indicates the ability of PDA to maintain the capacitance to a certain extent; however, after a trigger point, the PDA will loose the protective effect as shown in the sample DPS-1 case. The capacitance retention of sample DPS-2 shows much improved results than the sample DPS-1. It maintains as high as 94.6% after 2000 cycles. This strongly indicates that the content or thickness of PDA coating onto the PANI-SWCNT composite material is a crucial parameter to obtain the stability of the overall electrochemical activity.

For the degradation of PANI during electrochemcial cycling, there are two possible degradation pathways. The first one is mechanical degradation, where PANI simply detaches from the substrate. The other one is chemical degradation, which is often the result of over oxidation or over reduction.[12,13] To investigate the degradation mechanism in the sample PS and sample DPS-2, attenuated total reflectance (ATR) FTIR tests were carried out on sample loaded graphite paper before and after cycling tests. The results are shown in Fig. 7. The samples before cycling show the identical FTIR spectra resembling the corresponding samples in Fig. 3. The samples after cycling show two distinct differences in the FTIR spectra. As indicated by red triangles and blue circles, there is an additional C=O stretching in phenyl or vinyl esters.[38,39] Meanwhile, it also can be observed that the C–H out-of-plane vibration in aromatic rings from around 830 to 800 cm^{-1} have diminished after cycling. Combining this information, there should be a certain chemical oxidation of PANI during long term cycling tests in the 1 M $LiClO_4$ in PC. However, such a transition is hard to quantitatively study. Based on the capacitance retention information in Fig. 5(b), the chemical degradation of PANI would not lead to such a drop in the capacitance in the long-term cycling. The SEM images of sample PS before and after cycling are shown in Fig. S3 (supporting information). It could be clearly observed that there is a certain degree of active material peeling off from the SWCNTs, as indicated by the red arrows in Fig. S3(f). Therefore, it could be deduced that the mechanical degradation is probably the most important factor for the degradation of the electrochemical performance. Otherwise, the sample DPS-2 should undergo a huge decrease in capacitance as well.

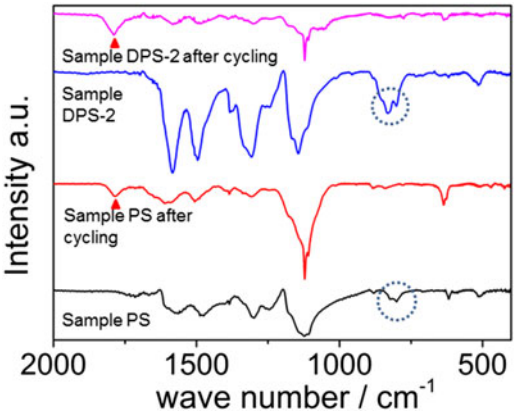


FIG. 7. ATR FTIR spectra of sample PS and sample DPS-2 on graphite paper before and after the cycling test.

IV. CONCLUSION

In summary, we investigated the electrochemical energy storage application of PANI-SWCNT based composites for organic electrolyte based supercapacitors. PANI-SWCNT composites were able to deliver high specific capacitance with reasonable rate capability. The capacitance and cycling stability of the PANI-SWCNT composite can be further improved by controlled PDA modification. Mechanical degradation (active material peeling off) was found to be the primary reason for PANI electrode degradation during electrochemical cycling. The PDA modification enhanced the adhesion to the current collector so as to achieve better cycling stability in the organic electrolyte for the PANI-SWCNT composite. The PDA modified PANI-SWCNT is a promising replacement for carbon materials as a cathode in organic electrolyte based supercapacitors. It would be interesting to further investigate future high voltage and high energy density supercapacitors based on PDA modified PANI-SWCNTs.

ACKNOWLEDGMENT

This research is supported by NRF Competitive Research Program NRF-CRP13-2014-02. Part of the work was carried out in the NTU-HUJ-BGU Nanomaterials for Energy and Water Management Program under the Campus for Research Excellence and Technological Enterprise (CREATE), that is supported by the National Research Foundation, Prime Minister's Office, Singapore.

REFERENCES

1. C. Liu, F. Li, L.P. Ma, and H.M. Cheng: Advanced materials for energy storage. *Adv. Mater.* **22**(8), E28 (2010).
2. A. Du Pasquier, I. Plitz, S. Menocal, and G. Amatucci: A comparative study of Li-ion battery, supercapacitor and non-aqueous asymmetric hybrid devices for automotive applications. *J. Power Sources* **115**(1), 171 (2003).
3. A. Burke: R&D considerations for the performance and application of electrochemical capacitors. *Electrochim. Acta* **53**(3), 1083 (2007).
4. K. Naoi, S. Ishimoto, J-i. Miyamoto, and W. Naoi: Second generation 'nanohybrid supercapacitor': Evolution of capacitive energy storage devices. *Energy Environ. Sci.* **5**(11), 9363 (2012).
5. V. Aravindan, J. Gnanaraj, Y-S. Lee, and S. Madhavi: Insertion-type electrodes for nonaqueous Li-ion capacitors. *Chem. Rev.* **114**(23), 11619 (2014).

https://doi.org/10.1557/jmr.2015.342 Published online by Cambridge University Press

6. L.L. Zhang and X. Zhao: Carbon-based materials as supercapacitor electrodes. *Chem. Soc. Rev.* **38**(9), 2520 (2009).
7. V. Augustyn, P. Simon, and B. Dunn: Pseudocapacitive oxide materials for high-rate electrochemical energy storage. *Energy Environ. Sci.* **7**(5), 1597 (2014).
8. B. Kim, H. Chung, and W. Kim: High-performance supercapacitors based on vertically aligned carbon nanotubes and nonaqueous electrolytes. *Nanotechnology* **23**(15), 155401 (2012).
9. V. Gupta and N. Miura: Polyaniline/single-wall carbon nanotube (PANI/SWCNT) composites for high performance supercapacitors. *Electrochim. Acta* **52**(4), 1721 (2006).
10. K. Wang, P. Zhao, X. Zhou, H. Wu, and Z. Wei: Flexible supercapacitors based on cloth-supported electrodes of conducting polymer nanowire array/SWCNT composites. *J. Mater. Chem.* **21**(41), 16373 (2011).
11. A. Sumboja, U.M. Tefashe, G. Wittstock, and P.S. Lee: Investigation of charge transfer kinetics of polyaniline supercapacitor electrodes by scanning electrochemical microscopy. *Adv. Mater. Interfaces* **2**(1), 1400154 (2015).
12. E. Song and J-W. Choi: Conducting polyaniline nanowire and its applications in chemiresistive sensing. *Nanomaterials* **3**(3), 498 (2013).
13. J. Yan, L. Yang, M. Cui, X. Wang, K.J. Chee, V.C. Nguyen, V. Kumar, A. Sumboja, M. Wang, and P.S. Lee: Aniline tetramer-graphene oxide composites for high performance supercapacitors. *Adv. Energy Mater.* **4**(18), 1400781 (2014).
14. H. Lee, S.M. Dellatore, W.M. Miller, and P.B. Messersmith: Mussel-inspired surface chemistry for multifunctional coatings. *Science* **318**(5849), 426 (2007).
15. J. Yan, L. Yang, M.F. Lin, J. Ma, X. Lu, and P.S. Lee: Polydopamine spheres as active templates for convenient synthesis of various nanostructures. *Small* **9**(4), 596 (2013).
16. J.H. Hafner, M.J. Bronikowski, B.R. Azamian, P. Nikolaev, A.G. Rinzler, D.T. Colbert, K.A. Smith, and R.E. Smalley: Catalytic growth of single-wall carbon nanotubes from metal particles. *Chem. Phys. Lett.* **296**(1–2), 195 (1998).
17. M.E. Lynge, R. van der Westen, A. Postma, and B. Städler: Polydopamine—a nature-inspired polymer coating for biomedical science. *Nanoscale* **3**(12), 4916 (2011).
18. T. Abdiryim, Z. Xiao-Gang, and R. Jamal: Comparative studies of solid-state synthesized polyaniline doped with inorganic acids. *Mater. Chem. Phys.* **90**(2–3), 367 (2005).
19. M. Trchová, I. Šeděnková, E. Tobolková, and J. Stejskal: FTIR spectroscopic and conductivity study of the thermal degradation of polyaniline films. *Polym. Degrad. Stab.* **86**(1), 179 (2004).
20. W. Zheng, M. Angelopoulos, A.J. Epstein, and A.G. MacDiarmid: Experimental evidence for hydrogen bonding in polyaniline: mechanism of aggregate formation and dependency on oxidation state. *Macromolecules* **30**(10), 2953 (1997).
21. R.A. Zangmeister, T.A. Morris, and M.J. Tarlov: Characterization of polydopamine thin films deposited at short times by autoxidation of dopamine. *Langmuir* **29**(27), 8619 (2013).
22. C. Peng, D. Hu, and G.Z. Chen: Theoretical specific capacitance based on charge storage mechanisms of conducting polymers: Comment on 'Vertically oriented arrays of polyaniline nanorods and their super electrochemical properties'. *Chem. Commun.* **47**(14), 4105 (2011).
23. K. Zhang, L.L. Zhang, X.S. Zhao, and J. Wu: Graphene/polyaniline nanofiber composites as supercapacitor electrodes. *Chem. Mater.* **22**(4), 1392 (2010).
24. C-C. Hu and J-Y. Lin: Effects of the loading and polymerization temperature on the capacitive performance of polyaniline in $NaNO_3$. *Electrochim. Acta* **47**(25), 4055 (2002).
25. S.R. Sivakkumar, J-S. Oh, and D-W. Kim: Polyaniline nanofibres as a cathode material for rechargeable lithium-polymer cells assembled with gel polymer electrolyte. *J. Power Sources* **163**(1), 573 (2006).
26. S. Ardizzone, G. Fregonara, and S. Trasatti: INNER and outer active surface of RUO_2 electrodes. *Electrochim. Acta* **35**(1), 263 (1990).
27. X. Petrissans, A. Betard, D. Giaume, P. Barboux, B. Dunn, L. Sicard, and J.Y. Piquemal: Solution synthesis of nanometric layered cobalt oxides for electrochemical applications. *Electrochim. Acta* **66**, 306 (2012).
28. M. Sathiya, A.S. Prakash, K. Ramesha, J.M. Tarascon, and A.-K. Shukla: V_2O_5-anchored carbon nanotubes for enhanced electrochemical energy storage. *J. Am. Chem. Soc.* **133**(40), 16291 (2011).
29. G.A. Snook, P. Kao, and A.S. Best: Conducting-polymer-based supercapacitor devices and electrodes. *J. Power Sources* **196**(1), 1 (2011).
30. W.J. Albery, Z. Chen, B.R. Horrocks, A.R. Mount, P.J. Wilson, D. Bloor, A.T. Monkman, and C.M. Elliott: Spectroscopic and electrochemical studies of charge transfer in modified electrodes. *Faraday Discuss. Chem. Soc.* **88**, 247 (1989).
31. B.E. Conway: *Electrochemical Supercapacitors: Scientific Fundamentals and Technological Applications* (Kluwer Academic/Plenum, New York, 1999).
32. X. Wang, W.S. Liu, X. Lu, and P.S. Lee: Dodecyl sulfate-induced fast faradic process in nickel cobalt oxide-reduced graphite oxide composite material and its application for asymmetric supercapacitor device. *J. Mater. Chem.* **22**(43), 23114 (2012).
33. J. Liebscher, R. Mrówczyński, H.A. Scheidt, C. Filip, N.D. Hădade, R. Turcu, A. Bende, and S. Beck: Structure of polydopamine: A never-ending story? *Langmuir* **29**(33), 10539 (2013).
34. M. Beidaghi and C.L. Wang: Micro-supercapacitors based on interdigital electrodes of reduced graphene oxide and carbon nanotube composites with ultrahigh power handling performance. *Adv. Funct. Mater.* **22**(21), 4501 (2012).
35. P.L. Taberna, P. Simon, and J.F. Fauvarque: Electrochemical characteristics and impedance spectroscopy studies of carbon-carbon supercapacitors. *J. Electrochem. Soc.* **150**(3), A292 (2003).
36. M. Kaempgen, C.K. Chan, J. Ma, Y. Cui, and G. Gruner: Printable thin Film supercapacitors using single-walled carbon nanotubes. *Nano Lett.* **9**(5), 1872 (2009).
37. Y. Liu, K. Ai, and L. Lu: Polydopamine and its derivative materials: Synthesis and promising applications in energy, environmental, and biomedical fields. *Chem. Rev.* **114**(9), 5057 (2014).
38. N. Betz, A. Le Moël, E. Balanzat, J.M. Ramillon, J. Lamotte, J.P. Gallas, and G. Jaskierowicz: A FTIR study of PVDF irradiated by means of swift heavy ions. *J. Polym. Sci., Part B: Polym. Phys.* **32**(8), 1493 (1994).
39. C.A. Pryde: IR studies of polyimides. I. Effects of chemical and physical changes during cure. *J. Polym. Sci., Part A: Polym. Phys.* **27**(2), 711 (1989).

Supplementary Material

To view supplementary material for this article, please visit http://dx.doi.org/jmr.2015.342.

https://doi.org/10.1557/jmr.2015.342 Published online by Cambridge University Press